

Pressure anisotropy and B_y in the magnetotail current sheet

Richard L. Kaufmann, Bryan M. Ball

Department of Physics, University of New Hampshire, Durham

W. R. Paterson and L. A. Frank

Department of Physics and Astronomy, University of Iowa, Iowa City

Abstract. Ions were almost isotropic at the neutral sheet throughout the $(-31 < x < -7 R_E)$, $(0 < |y| < 15 R_E)$ region studied using Geotail data. Pressure anisotropies developed in the middle and outer current sheet, indicating the influence of nonguiding center motion or parallel electric fields. The pressure anisotropies were only large enough to provide from 10% to 30% of the force needed to balance the $\mathbf{j} \times \mathbf{B}$ force.

The sign of the measured B_y was used to find where magnetic field fluctuations and the influence of the IMF B_y dominate over the long term averaged B_y . The fluctuation and IMF effects dominated throughout the current sheet near midnight and near the neutral sheet away from midnight. The average fluctuation plus IMF influence produced a 2 to 3 nT contribution to B_y in the low and mid β regions near midnight and a 1 to 2 nT contribution to B_y in the highest β region. Since shielding of these contributions to B_y was found to be weak, this suggests that any IMF effect most likely distorts the current sheet rather than generating a steady field in the plane of the neutral sheet. The lack of shielding also suggests that fluctuations have scale lengths on the order of an ion gyroradius or less.

1. Introduction

This paper is part of a project to study the structure of the current sheet in the magnetotail. Calculations using a consistent orbit tracing (COT) method [Larson and Kaufmann, 1996] are being compared with distribution functions and plasma moments measured by the Geotail com-

prehensive plasma instrumentation [Frank *et al.*, 1994] and with data from the Geotail magnetic field experiment [Kokubun *et al.*, 1994]. An evaluation of each term in the momentum and energy equations will be presented elsewhere. The present report describes alternate ways to study several features of the plasma sheet. The goal is to get a better understanding of magnetotail structure by looking at observations from different viewpoints. The specific topics discussed here involve ion pressure anisotropy and the combined influence of fluctuations plus the IMF on measurements of B_y in the plasma sheet.

One-minute averages of Geotail data taken between Jan. 31, 1995 and Mar. 1, 1996 were used. Paterson *et al.* [1998] averaged several fluid parameters for a period that included the interval used here. Only the 104,000 data points taken at $|y| < 15 R_E$ in aberrated GSE coordinates were considered to assure that the measurements were inside the magnetosphere. A 4.5° aberration correction was made to account for the motion of the Earth around the Sun [Troshichev *et al.*, 1999]. Data points then were removed if the count rate was very low. This criterion eliminated many of the lobe observations. Data points also were removed if the measured ion and electron densities differed by more than a factor of two, indicating a problem with determinations of the satellite potential or photoelectron corrections. Several other checks were made, but they removed only a small number of suspicious data points. The remaining 90,000 1-minute averages were used for the analysis.

2. Ion pressure anisotropy

Two fluid parameters are examined in this section. The first shows that plasma within the current sheet does not behave as would be expected using the MHD or guiding center approximations. The second parameter provides some information about force balance.

Figure 1 shows how the ion pressure anisotropy varies in the middle magnetotail. The ion P_{\parallel}/P_{\perp} measurements were sorted into $3 R_E \times 3 R_E$ x - y boxes. Similar patterns were seen on the

dawn and dusk sides so the results at (x, y) and $(x, -y)$ were combined to reduce the number of plots and to increase the amount of data in each plot. Centers of the five different y -boxes are listed at the top of the Figure. There are eight x -boxes in the $-31 < x < -7 R_E$ region studied. Two curves, showing data at the two adjacent x -locations listed along the right edge of Figure 1, are plotted in each of the four rows of panels. The solid line is for the x -box that is farther from Earth. For example, the solid curve in the top row represents $-31 < x < -28 R_E$ and the dotted curve in the top row is for the $-28 < x < -25 R_E$ box.

Data in each x - y box also has been sorted according to plasma beta or the ratio of the thermal particle energy density to the magnetic field energy density. The horizontal axis of each panel in Figure 1 is the β -box number, with the beta ranges listed in the Figure caption. Sorting by β is used to remove effects of tail distortion and motion such as flapping, warping, and twisting. The largest beta, which is expected to correspond to the smallest $|z|$ or distance from the neutral sheet, is at the left side of each panel. The smallest beta, corresponding to the largest $|z|$, is at the right side of each panel. The β -box number therefore is used as a nonlinear and presently uncalibrated measure of the instantaneous distance from the satellite to the neutral sheet.

There usually were fewer than 50 data points in β -boxes 1, 7, and 8. Beta-boxes 7 and 8 had few data points because the minimum count rate criterion eliminated 30% and 80% of the measurements in these boxes, respectively. The removal of so much data can produce systematic errors and the erratic behavior that is apparent in these boxes. Fewer than 2% of the measurements were removed from β -boxes 1 to 5 and 8% were removed from box 6 as a result of the low count rate cutoff. The small number of points in β -box 1 also can produce large uncertainties, but simply represents the fact that β rarely exceeds 30. Beta boxes 3 to 5 usually contained about 200 points on each the dawn and dusk sides.

Almost every curve throughout the region studied in Figure 1 shows P_{\parallel}/P_{\perp} near 1.0 in β boxes 1 and 2, indicating that ions are almost isotropic near the neutral sheet. Figure 1 also shows

that P_{\parallel}/P_{\perp} averages about 1.1 to 1.2 in the outer current sheet beyond $x = -13 R_E$, where the magnetic field structure is tail-like. The average B_z is less than 5 nT beyond $x = -13 R_E$ and B_z increases rapidly to between 10 and 15 nT in the most earthward two x -boxes, indicating the transition to a dipolar geometry. The plots in this paper were prepared using the uncorrected Geotail magnetic field data. A revised data set with B_z reduced by 0.5 ± 0.3 nT is expected to be available in the near future (S. Kokubun, personal communication, 1999). Sets of plots similar to those shown here have been run with approximate magnetic field corrections. The expected revision produced only minor changes in Figure 1.

Errors are difficult to estimate because the assumption that the 1-minute averages can be treated as a random sampling drawn from a normal distribution is invalid for many fluid parameters. The satellite entered each $3 R_E \times 3 R_E$ x - y box only about 10 times per year. Individual β -boxes within each x - y box therefore were entered only a few times. Some fluid parameters remain relatively steady while the satellite passes through a box. The standard deviation of individual data points was calculated for each x - y - β box in Figure 1. Most of these standard deviations of the P_{\parallel}/P_{\perp} ratio were between 0.1 and 0.2 when $\beta > 0.3$, and they increased to an average of nearly 0.5 for β -box 8. An estimate of the standard error of the curves in Figure 1 derived by dividing the standard deviation by $(N - 1)^{1/2}$ and using the number of 1-minute averages for N gives an estimated error of between 0.01 and 0.02 for $\beta > 0.3$. This error estimate increases to an average of nearly 0.1 for β -box 8. An examination of the box-to-box fluctuations in Figure 1 shows that these estimates are much too small, and that something between the number of data points and the number of times a box was entered should be used for N to estimate errors. The best way to treat uncertainties is probably to compare separate plots made using different data sets. Lacking this, the box-to-box fluctuations seen in plots such as Figure 1 provide a reasonable estimate of the statistical errors.

One significant conclusion that can be drawn from Figure 1 is that nonguiding center effects

or parallel electric fields are important in the inner current sheet. The fact that P_{\parallel}/P_{\perp} increases from 1.0 near the neutral sheet to 1.1 or 1.2 in the outer current sheet throughout the large region studied shows that the pressure anisotropy increases as one moves along field lines away from the neutral sheet. Similar features have been noted in orbit tracing studies using nonguiding center particles. In contrast, the pressure would remain isotropic and constant along a field line in the guiding center approximation if pressure was isotropic at the equator and if $E_{\parallel} = 0$.

Figure 2 shows the closely related fire hose instability parameter $[P_{\parallel} - P_{\perp}]/[B^2/\mu_o]$. The fire hose parameter would be 1.0 at the outer edge of the current sheet if the tailward centrifugal force associated with the change in v_x from tailward to earthward during each current sheet interaction was equal to the earthward $\mathbf{j} \times \mathbf{B}$ force [Rich *et al.*, 1972; Cowley, 1978; Schindler, 1979]. The parameter plotted in Figure 2 was obtained using β -box averages of P_{\parallel} , P_{\perp} and B^2 in the above expression. This was done because a single 1-minute point can give an extremely large value of the fire hose parameter if B is nearly zero. One or a few points therefore tended to dominate the averages in the first few β -boxes, where B is smallest, when the parameter was calculated separately for each 1-minute interval and then averaged. The fire hose parameter also depends very sensitively upon small errors in the magnetic field data in weak field regions. Since both the numerator and denominator of the fire hose parameter approach zero in β -box 1, results for this box are especially unreliable. The standard deviation of the fire hose parameter decreased from 1 in β -box 2 to 0.1 in box 5 and 0.01 in box 8. The estimated errors of the curves in Figure 2 derived using the number of 1-minute averages for N are 0.1 for β -box 2, 0.01 for box 4, and 0.003 for boxes 6 through 8. These estimates again are unrealistically small, and a better estimate is obtained by simply observing the box-to-box variations.

The fire hose parameter in Figure 2 peaks near 0.1 somewhere in the inner current sheet throughout the tail-like region. Excluding β -boxes 1 and 2, a plot similar to Figure 2 but using the average of the fire hose parameter calculated separately for each 1-minute data point peaks near

0.2. The anticipated magnetic field correction and the low ion count rates both suggest that the fire hose parameter may be underestimated at the outer edge of the principal current sheet. These results indicate that the earthward acceleration of ions as they cross the equator requires only $20\% \pm 10\%$ of the $\mathbf{j} \times \mathbf{B}$ force. Pressure variations in the x direction balance a larger portion of the earthward force and a small residual force imbalance is needed to explain the variations in average bulk velocity as plasma drifts earthward. A more complete study of force balance including effects of each element of the pressure tensor will be presented elsewhere.

3. Influence of fluctuations and of the IMF on the magnetotail B_y

Most studies of the influence of the interplanetary magnetic field (IMF) on the tail have involved direct correlations of measurements made in the solar wind or magnetosheath with measurements made in the magnetotail. *Kaymaz et al.* [1994] presented IMP 8 observations and summarized results from several earlier analyses. These studies revealed significant correlations between the IMF B_y and the magnetotail field. The correlation is sometimes discussed in terms of the penetration of a fraction of the IMF B_y into the plasma sheet. Large fluctuations also are commonly seen in the tail magnetic field [*Borovsky et al.*, 1997]. In some regions it is possible for fluctuations or effects of the IMF to dominate over the long term averaged field in determining the sign of the 1-minute averaged B_y . The long term averaged field includes contributions from the steady ring, tail, Birkeland, and magnetopause current systems as well as the Earth's dipole field [*Tsyganenko*, 1989; *Tsyganenko and Stern*, 1996]. This section presents a different way to study B_y effects and is based only on Geotail data.

Figure 3 shows the 1-year averages of B_x and B_y measured when Geotail was at the outer edge of the current sheet. Magnetic field data were rotated by 4.5° so that B_y approximately equals the field in the aberrated GSE y direction. A total of 12,000 data points fell into the $(0.1 < \beta < 0.3)$ boxes. The signs of both B_x and B_y were reversed whenever $B_x < 0$ in order to combine data from

north and south of the neutral sheet. Since the observed B_y is antisymmetric across the $y = 0$ plane, data taken at equal $|y|$ on the dawn and dusk sides also have been folded together for the following analysis by reversing the sign of B_y for all data taken at $y < 0$. The B_y effects therefore will be described as if all measurements were taken in the northern dusk quadrant. The average folded B_y beyond $x = -13 R_E$ in Figure 3 is -0.4 nT in the $0 < |y| < 3 R_E$ boxes and -5 nT in the $12 < |y| < 15 R_E$ boxes. Averaging over a full year removes nearly all effects of fluctuations and the IMF B_y because the sign of B_y is reversed whenever the satellite is in two quadrants and because fluctuations and the IMF are roughly equally likely to produce positive and negative B_y effects. Figure 3 therefore gives an approximation of the steady portion of the tail field, and is similar to the empirical models [Tsyganenko, 1989; Tsyganenko and Stern, 1996].

Magnetization currents shield steady x and y components of the magnetic field from the high β inner current sheet if the current sheet lies in the x - y plane. In the MHD approximation magnetization currents are produced by the circular motion of particles about stationary guiding centers [Parker, 1957]. Such currents are associated with pressure gradients and magnetic field line curvature. Magnetization currents carried by nonguiding center particles are easiest to study in one-dimensional magnetic field models because trapped particles have no net drift in such a field. Kaufmann and Lu [1993] described the importance of magnetization currents in the construction of a model current sheet using nonguiding center particles. Magnetization current flows from dusk to dawn at the neutral sheet and from dawn to dusk in the outer current sheet in a magnetotail with $B_y = 0$. This current system reduces B_x in the current sheet from its maximum value which is found in the lobes. Figure 4 shows how complete this shielding is for the $\beta > 10$ or neutral sheet region. A total of 12,000 data points fell into the $\beta > 10$ boxes. The average folded B_y beyond $x = -13 R_E$ in Figure 4 is between -0.5 and 0.2 nT in the various $|y|$ boxes. Note that the magnetic field scale changes by a factor of four between Figures 3 and 4. Since magnetization currents are generated by orbital motion in whatever field is present, any relatively steady contribution of the

IMF to the magnetic field in the plane of the current sheet should also be shielded near the neutral sheet.

Figure 5 shows one way to examine the influence of fluctuations and of the IMF B_y . The ratio $-B_y/|B_y|$ for each 1-minute data point equals +1 whenever the measured B_y is negative and -1 whenever B_y is positive. Since all data has been folded into the northern dusk quadrant, each 1-minute point with B_y pointing in the direction shown in Figure 3 produces $-B_y/|B_y| = +1$. The 1-year averages of this ratio would equal +1 if the long term averaged field always determined the sign of B_y . At the other extreme, if fluctuations and the influence of the IMF B_y were always so strong that they dominated the measured B_y then the above ratio would be +1 half the time and -1 the other half. The 1-year average of the $-B_y/|B_y|$ ratio therefore should be near zero in regions where fluctuations or the IMF B_y dominates. The incorporation of other data would permit a separation of the effects of fluctuations from the effects of the IMF B_y , but the present analysis does not distinguish between these two possible causes of a reversal in the sign of B_y .

Figure 5 shows the 1-year average of the 1-minute $-B_y/|B_y|$ ratio. Most of the observations in the tail-like region show that the long term averaged field nearly always dominates in the outer current sheet and lobe well away from midnight ($|y| > 6 R_E$). Figure 5 also shows that the ratio fluctuates about zero in the tail-like region at $|y| < 3 R_E$, indicating that fluctuations or the IMF almost always dominates in determining the sign of B_y near midnight. A comparison with Figure 3 shows that these qualitative results are not surprising. The long term averaged B_y is nearly zero at midnight so it is easiest for fluctuations or the IMF to dominate.

Since the $-B_y/|B_y|$ ratio always equals ± 1 its standard deviation has little significance. The standard deviation of the folded B_y averages 1 nT in β -box 1, 2 nT in β -box 2, and 3 nT in β -boxes 3 through 7. The standard errors obtained if the number of 1-minute averages is used for N is between 0.1 and 0.2 nT for β -boxes 1 through 6. One useful conclusion from Figure 5 is that the transition to dominance by fluctuations or the IMF when $\beta < 1$ (β -boxes 5 to 8) takes place in the

$3 R_E < |y| < 6 R_E$ region. Another interesting feature of Figure 5 is that the $-B_y/|B_y|$ ratio is almost always small at the largest β (β -boxes 1 and 2) indicating that fluctuations or the IMF B_y dominates in the neutral sheet throughout the region studied. Therefore, even though a comparison of Figures 3 and 4 showed that the long term averaged B_x and B_y are shielded from the high β region, effects of fluctuations or the IMF B_y are not as well shielded.

While Figure 5 used only the sign of each 1-minute average of B_y to determine which source dominates, Figure 6 shows a way to study the influence of fluctuations and of the IMF B_y more quantitatively near midnight. The sum $B_y + |B_y|$ was calculated for each 1-minute period and this sum was then averaged over the 1-year study interval to create Figure 6. This parameter also has been folded to represent the northern dusk quadrant. For a single 1-minute point $B_y + |B_y|$ will be zero if B_y is negative and will equal $2 B_y$ if B_y is positive. The average of this sum therefore should equal zero in regions where fluctuations and the IMF never dominate because B_y will always be negative. Near midnight, where fluctuations and the IMF effects always dominate, it will be assumed that the effects of fluctuations or the IMF are positive half the time and negative half the time. The average $B_y + |B_y|$ then should equal twice the IMF plus fluctuation field half the time and zero the other half. As a result, curves in the $0 < |y| < 3 R_E$ boxes in Figure 6 provide an estimate of the fluctuation plus IMF associated contributions to B_y . The decrease away from midnight in the curves shown in Figure 6 reflect the fact that fluctuations are dominant less often in these x - y boxes.

Figure 6 shows that this average fluctuation plus IMF effect is between 2 and 3 nT in most of the plasma sheet in the tail-like region near midnight. The average IMF or fluctuating B_y appears to drop to between 1 and 2 nT in the highest β region (β -boxes 1 and 2) indicating possible weak shielding. Fluctuations would not be shielded by organized magnetization currents if their scale size was comparable to or smaller than the radius of curvature of a typical ion. Such fluctuations are likely to be frozen into and carried with the plasma in the high β region. If a relatively steady

uniform IMF B_y simply penetrated into the plasma sheet and altered the magnetic field in the plane of the neutral sheet, then this field would be expected to be shielded from the high β region along with the Earth's field. To remain unshielded, any IMF contribution to B_y therefore must primarily alter the shape of the plasma sheet through twisting or other distortions. The field normal to the neutral sheet is not well shielded by magnetization currents, which flow primarily in the plane of the current sheet. Any change in orientation will cause the normal field to have a y component in the satellite or GSE coordinate system.

4. Summary

This paper introduced a format for presenting some three-dimensional information about various parameters in a large section of the magnetotail. Separate panels were used to show measurements in each observation box in the x - y plane. The measurements in each x - y box were further sorted by β which was used as a nonlinear indicator of the instantaneous z location of the satellite relative to the neutral sheet. The satellite is assumed to be very close to the neutral sheet when $\beta > 10$ and to be in the outer current sheet or plasma sheet boundary layer when $0.1 < \beta < 1$.

The first measurements studied involved the ion pressure anisotropy or the closely related fire hose instability parameter. It was seen that pressure is almost fully isotropic at the neutral sheet and that anisotropies develop as one moves along a field line away from the equator. The development of anisotropies can be produced by nonguiding center motion of ions and by parallel electric fields. This result may be important to theoretical studies, simulations, and the projection of other measurements made well away from the neutral sheet. The pressure anisotropy was found to be too small at the edge of the current sheet to balance the earthward $\mathbf{j} \times \mathbf{B}$ force.

Another parameter studied was the y component of the magnetotail magnetic field. It was seen that the contribution by steady magnetospheric current systems to this field was shielded by magnetization currents. This long term averaged field has a negative B_y in the northern dusk side of the

plasma sheet. It was found that positive and negative observed B_y fields were almost equally likely at midnight and near the neutral sheet for all local times studied. This could either be an effect of fluctuations that are much larger than the long term averaged field in such regions or an effect of the IMF B_y . Individual satellite orbits can be found showing the temporary dominance of each B_y source. The amplitude of the average fluctuation or IMF B_y effect was about 2 to 3 nT near midnight throughout most of the plasma sheet and 1 to 2 nT very near the neutral sheet.

Acknowledgments. This material is based upon work supported by the National Science Foundation under grants ATM-9422056 and ATM-9730845 and by the National Aeronautics and Space Administration under grant NAG5-4453 at the University of New Hampshire. Research at the University of Iowa was supported by the National Aeronautics and Space Administration under grants NAG5-2371 and NAG5-7684. The authors would like to thank S. Kokubun who supplied full Geotail magnetic field measurements throughout the period studied. The reviewers also made a number of suggestions that are included in this paper.

References

- Borovsky, J. E., R. C. Elphic, H. O. Funsten, and M. F. Thomsen, The Earth's plasma sheet as a laboratory for flow turbulence in high- β MHD, *J. Plasma Phys.*, *57*, 1-34, 1997.
- Cowley, S. W. H., The effect of pressure anisotropy on the equilibrium structure of magnetic current sheets, *Planet. Space Sci.*, *26*, 1037-1061, 1978.
- Frank, L. A., K. L. Ackerson, W. R. Paterson, J. A. Lee, M. R. English, and G. L. Pickett, The comprehensive plasma instrumentation (CPI) for the GEOTAIL spacecraft, *J. Geomag. Geoelectr.*, *46*, 23-37, 1994.
- Kaufmann, R. L., and C. Lu, Cross-tail current: Resonant orbits, *J. Geophys. Res.*, *98*, 15,447-15,465, 1993.
- Kaymaz, Z., G. L. Siscoe, N. A. Tsyganenko, and R. P. Lepping, Magnetotail views at $33 R_E$: IMP 8 magnetometer observations, *J. Geophys. Res.*, *99*, 8705-8730, 1994.
- Kokubun, S., T. Yamamoto, M. H. Acuna, K. Hayashi, K. Shiokawa, and H. Kawano, The Geotail magnetic field experiment, *J. Geomagn. Geoelectr.*, *46*, 7-21, 1994.
- Larson, D. J., and R. L. Kaufmann, Structure of the magnetotail current sheet, *J. Geophys. Res.*, *101*, 21,447-21,461, 1996.
- Parker, E. N., Newtonian development of the dynamical properties of ionized gases of low density, *Phys. Rev.*, *107*, 924-933, 1957.
- Paterson, W. R., L. A. Frank, S. Kokubun, and T. Yamamoto, Geotail survey of ion flow in the plasma sheet: Observations between 10 and $50 R_E$, *J. Geophys. Res.*, *103*, 11,811-11,825, 1998.
- Rich, F. J., V. M. Vasyliunas, and R. A. Wolf, On the balance of stresses in the plasma sheet, *J. Geophys. Res.*, *77*, 4670-4676, 1972.
- Schindler, K., Theories of tail structures, *Space Sci. Rev.*, *23*, 365-374, 1979.

Troshichev, O., S. Kokubun, Y. Kamide, A. Nishida, T. Mukai, and T. Yamamoto, Convection in the distant magnetotail under extremely quiet and weakly disturbed conditions, *J. Geophys. Res.*, *101*, 10,249-10,263, 1999.

Tsyganenko, N. A., A magnetospheric magnetic field model with a warped tail current sheet, *Planet. Space Sci.*, *37*, 5-20, 1989.

Tsyganenko, N. A. and D. P. Stern, Modeling the global magnetic field of the large-scale Birke-land current systems, *J. Geophys. Res.*, *101*, 27,187-27,198, 1996.

Figure Captions

Figure 1. The ion pressure anisotropy ratio P_{\parallel}/P_{\perp} is shown for the $(-31 < x < -7 R_E)$, $(0 < |y| < 15 R_E)$ region studied. Data were sorted into $3 R_E \times 3 R_E$ boxes in the x - y plane. The center of each y -box is listed along the top of the figure. Data from two adjacent x -boxes are included in each panel. The x -box locations are listed along the right side of the figure. The solid curve shows data from the more distant of the two x -boxes. Data in each x - y box was further sorted according to plasma beta. The horizontal axis in each panel is the β -box number. The ranges associated with each β -box are: 1) $\beta > 30$, 2) $10 < \beta < 30$, 3) $3 < \beta < 10$, 4) $1 < \beta < 3$, 5) $0.3 < \beta < 1$, 6) $0.1 < \beta < 0.3$, 7) $0.03 < \beta < 0.1$, 8) $\beta < 0.03$.

Figure 2. The fire hose instability parameter $[P_{\parallel} - P_{\perp}]/[B^2/\mu_0]$ is plotted in a format similar to that used in Figure 1.

Figure 3. The vectors show the measured average B_x and B_y in each x - y box in the outer current sheet. Data taken when $0.1 < \beta < 0.3$ were used to generate the averages.

Figure 4. Similar to Figure 3 except for the neutral sheet. Data with $\beta > 10$ were used. Note that the scale is different from the scale in Figure 3.

Figure 5. Average of the $-B_y/|B_y|$ ratio in the format used for Figure 1. This parameter should be near +1 when the long term averaged field dominates and near zero when either fluctuations or the IMF dominates in determining the sign of the measured B_y .

Figure 6. Average of $B_y + |B_y|$ for the data set. This parameter should be near zero when the long term averaged field dominates and should equal the $|B_y|$ generated by fluctuations or the IMF when these influences determine the sign of B_y .

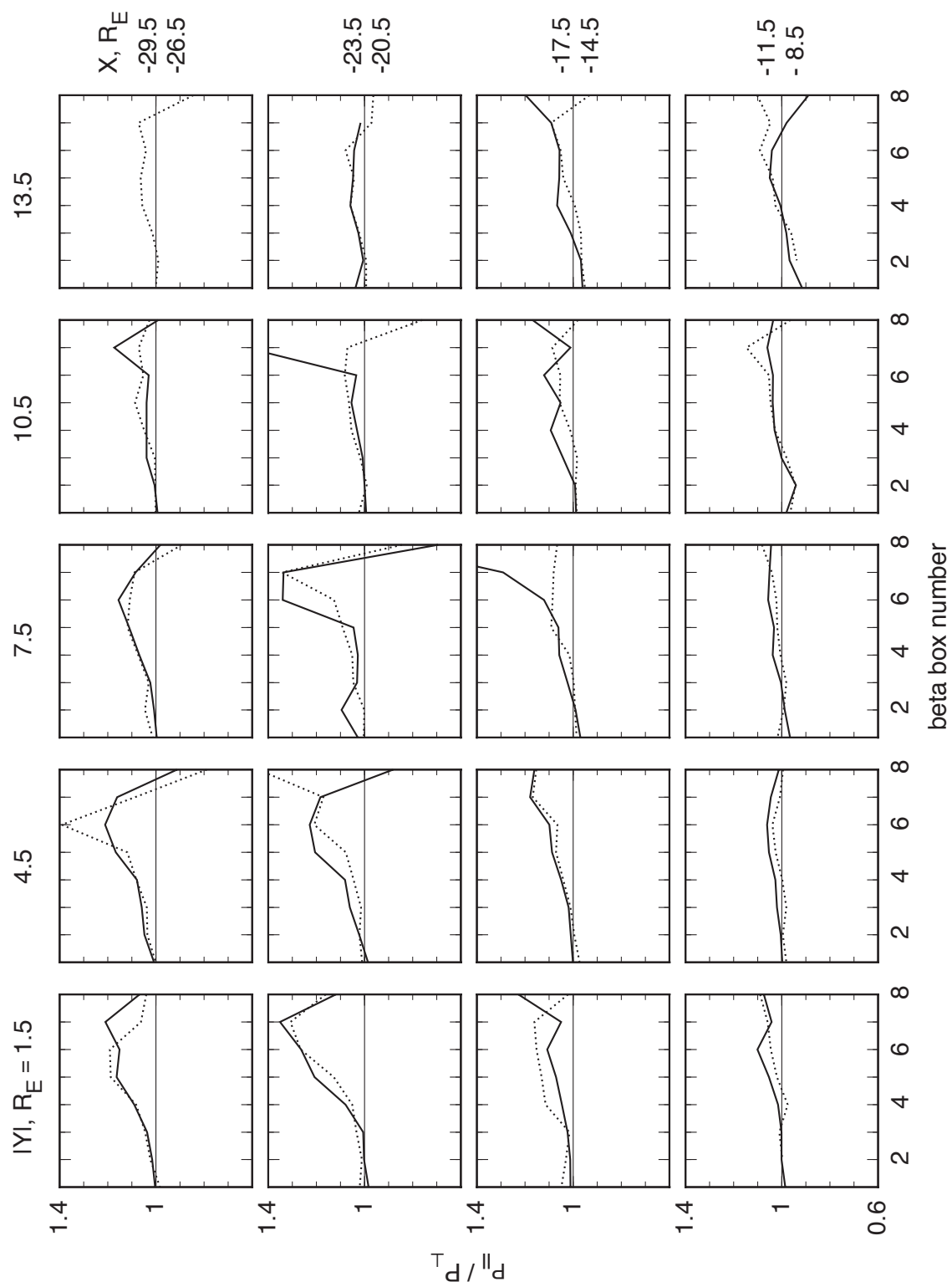


Figure 1

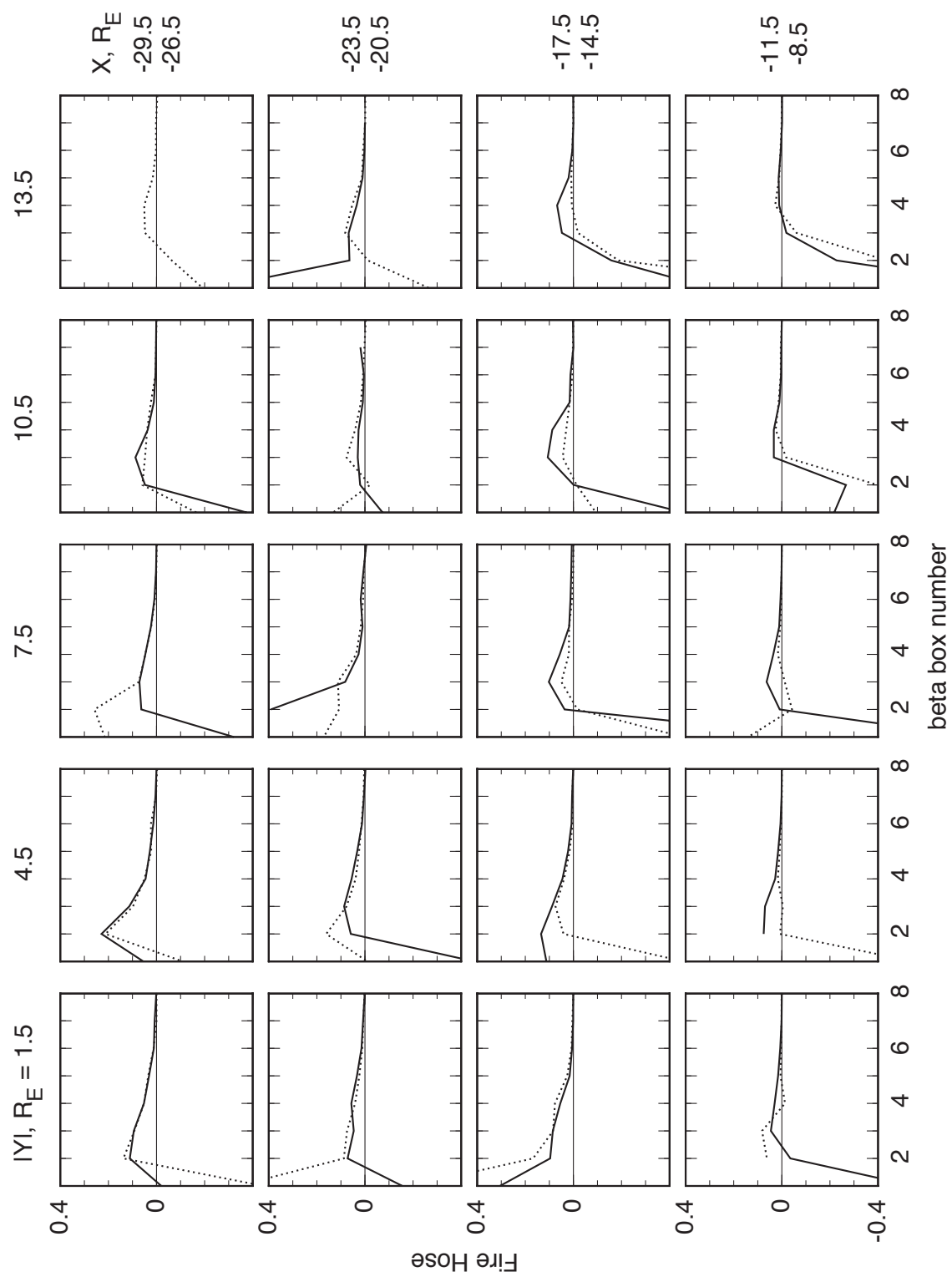


Figure 2

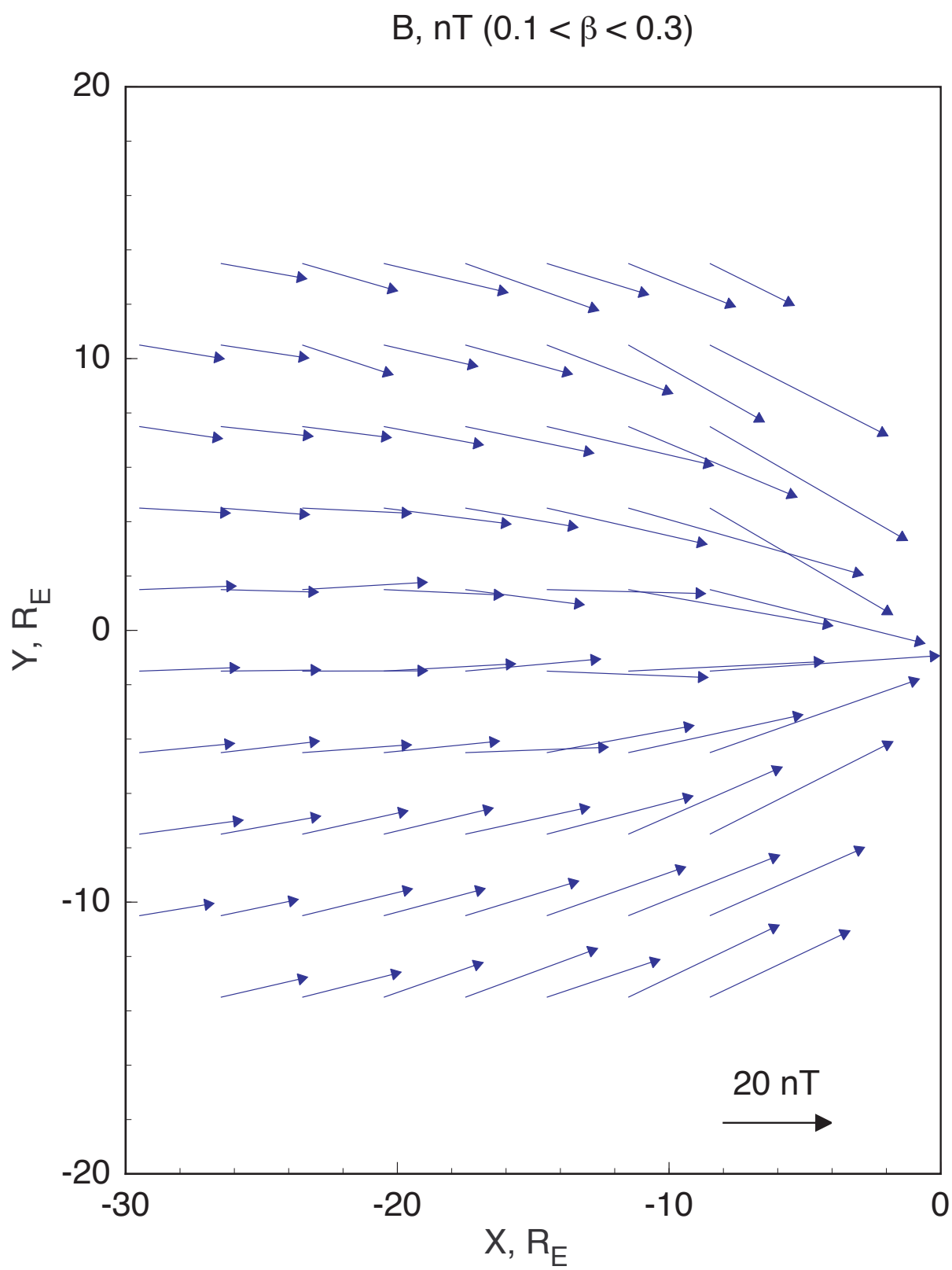


Figure 3

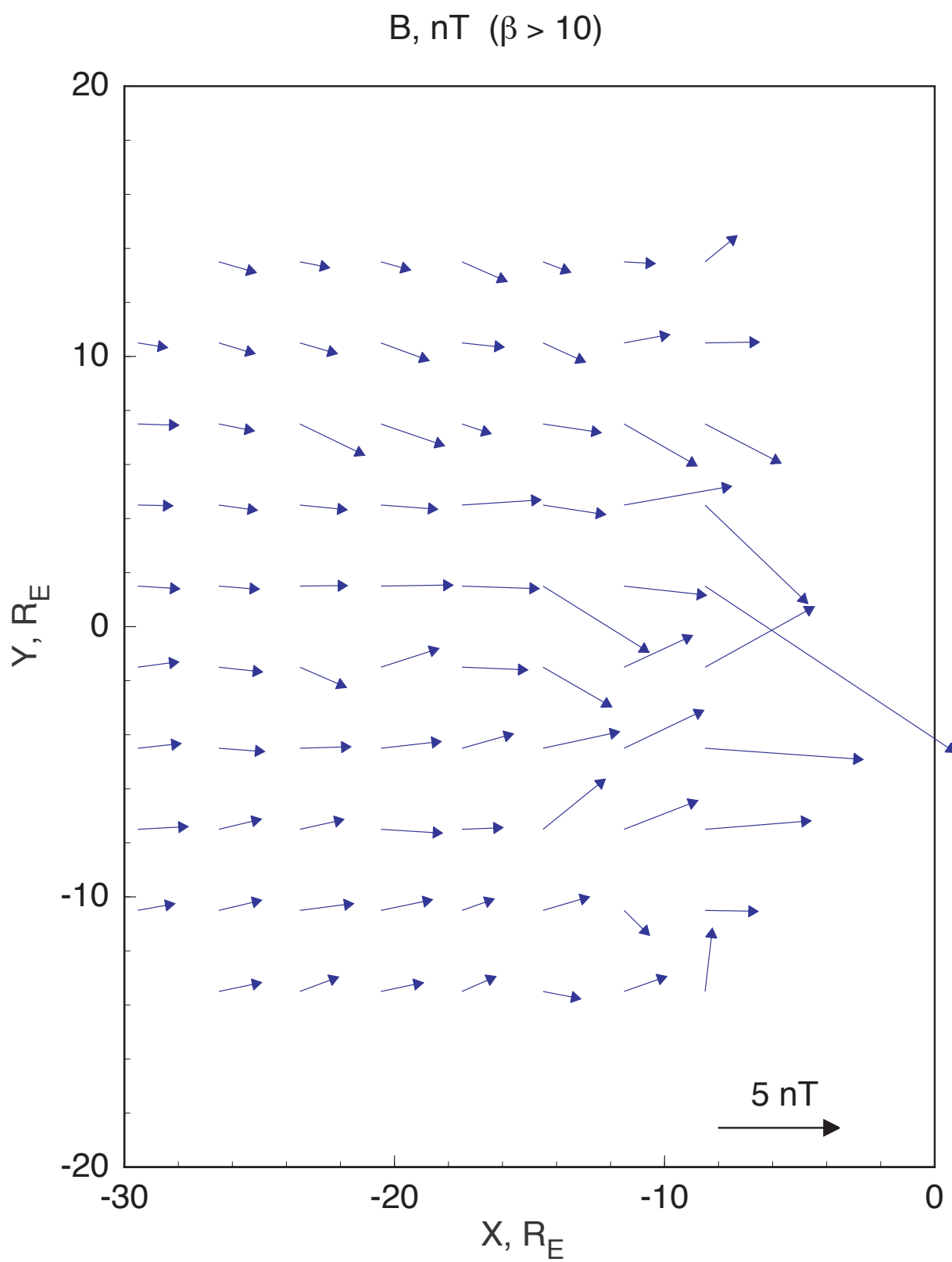


Figure 4

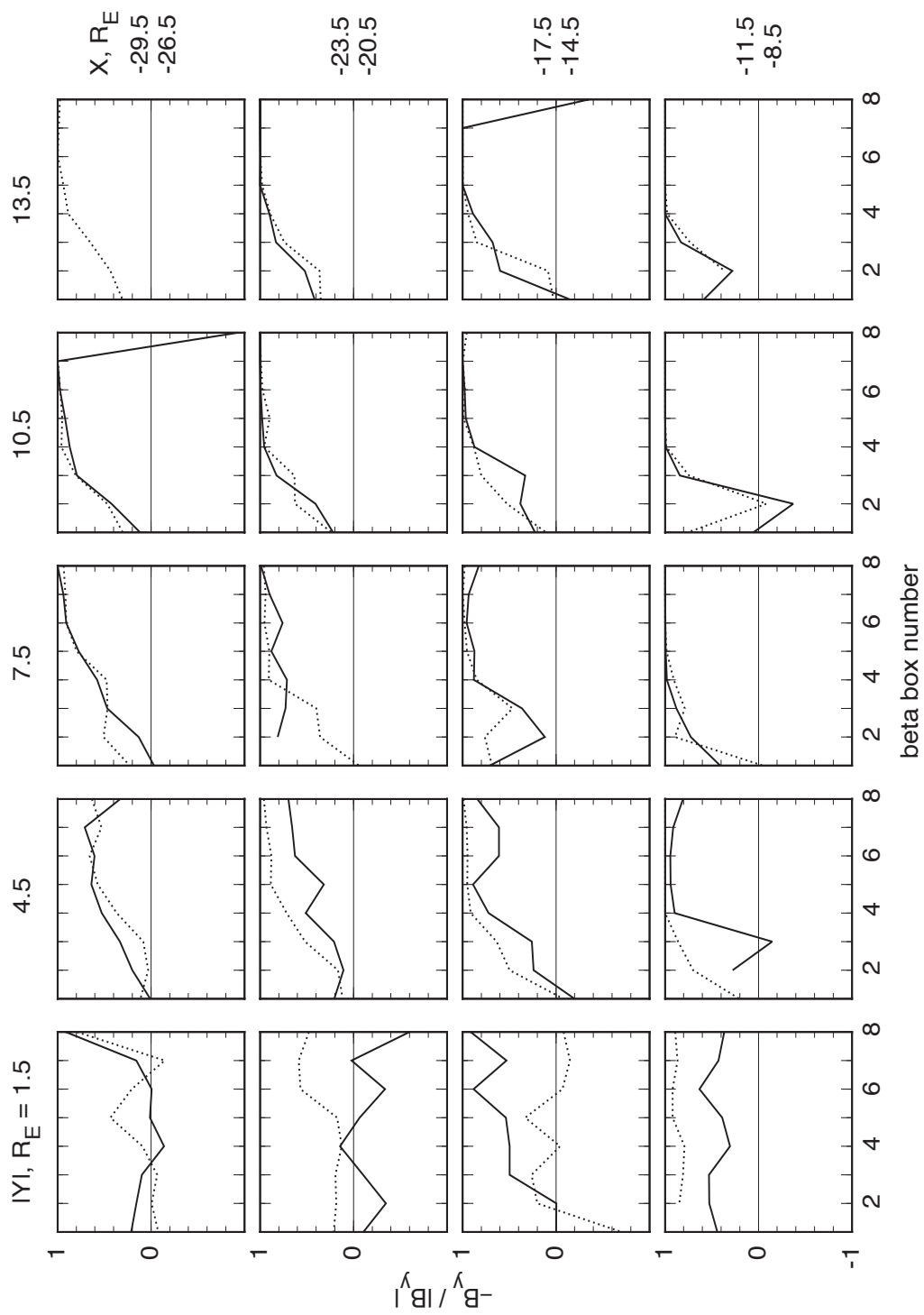


Figure 5

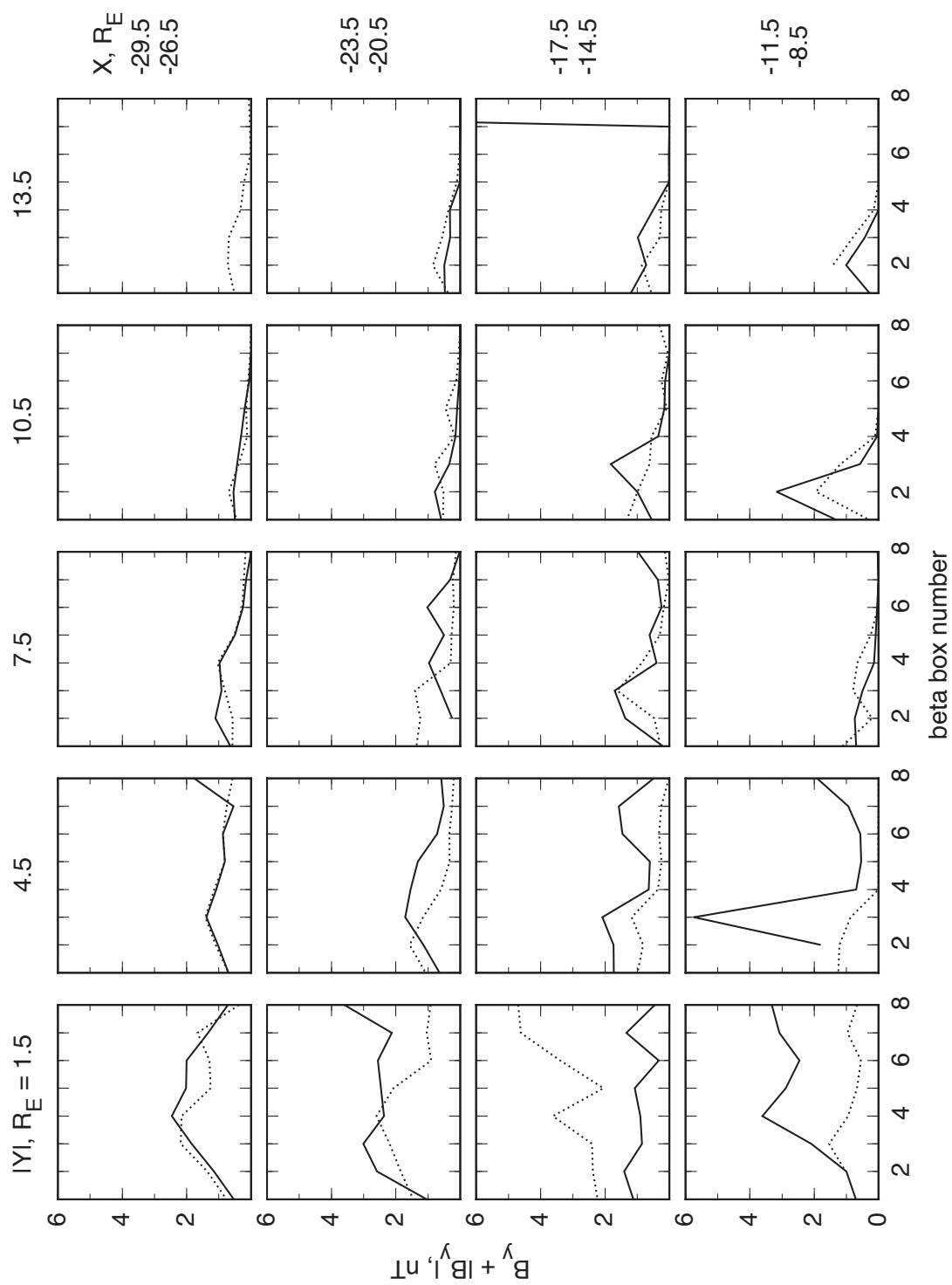


Figure 6